Electronic and chemical property of amorphous carbon, hydrocarbon, hydrogenated / hydrogen free carbon nitride: spectroscopic study

Sadhan Chandra Das[1-2], Abhijit Majumdar[2-3], and Rainer Hippler[2]

[1]UGC DAE CSR, Indore 452017, Khandwa road, MP, India

[2]Institute of Physics, University of Greifswald, Felix Hausdorff str 6, 17489 Greifswald, Germany

[3]Indian Institute of Engineering Science and Technology, Shibpur, Howrah-3, West Bengal, India

---

ABSTRACT: The comparative study of chemical properties and electronic bond structure of amorphous carbon (a-C), hydrocarbon (a-HC), carbon nitride (a-CN$_x$) and hydrogenated carbon nitride (a-HCN$_y$) is reported here. The spectroscopic analyses suggest that the presence of oxide layer is not only the prime cause but the presence of nitrogen is partially responsible for the chemical shift towards higher binding energy. In x-ray photoelectron spectroscopy (XPS), C 1s spectra of a-HCN$_y$ film shows higher chemical shifts compare to a-C, a-HC and a-CN$_x$. Raman spectra display a strong fluorescence effect of a-HC and a-HCN$_y$ where as a-C and a-CNx exhibits a promising G and D band at room temperature. Fourier transform infrared spectroscopy (FTIR) spectra show a large NH-OH over lapping region in a-HCN$_y$ compare to a-HC and a-CN$_x$ film whereas it is negligible in a-C. FTIR spectra show that the a-C, a-HC and a-CN$_x$ films are dominated by sp^2 bonded region while a-HCN$_y$ is the mixture of sp^2, sp^3 and hydrogen bridging bond.

KEYWORDS: Carbon nitride, Hydrogenated carbon nitride, Amorphous carbon, Hydrocarbon, Chemical shift, XPS, FTIR.

1 INTRODUCTION

The plasma assisted hydrocarbon film deposition is of considerable interest from both a fundamental and potential applications point of view because of its interesting chemical and structural properties [1, 2, 3]. The variety of processes have been employed to deposit hydrocarbon films and among of these techniques the rf plasma deposition is the most widely used [4, 5]. It is well established that the properties of a-C:H films may be adjusted over a wide range and that the most important deposition parameter is the ion energy [2, 3]. Amorphous carbon is a disordered phase of carbon without long-range order containing carbon atoms mostly in graphite-like sp^2 and diamond-like sp^3 hybridization states, and its physical properties depend strongly on the sp^2/sp^3 ratio. There are many forms of sp^2-bonded carbons with various degrees of graphitic ordering, ranging from microcrystalline graphite to glassy carbon [6].

In plasma assisted deposition of hydrocarbon films the low energy (<500 eV) species can induces various surface processes, such as surface activation, chemical sputtering, hydrogen release and synergisms between different species [7, 8]. Polymer-like hydrocarbon films can be deposited in remote areas of fusion devices when the growth process is dominated by surface reactions of reactive neutral species, such as hydrocarbon radicals [9, 10]. On the other hand, theoretical prediction regarding the mechanical properties of β-C$_3$N$_4$ solids to those of diamond [11] attracted a great interest of research towards carbon–nitrogen composite materials. Synthesis and outstanding mechanical properties of C$_3$N$_4$ was claimed by Marton et al. [12] but still there is no conclusive evidence about the possibility of synthesizing such super hard crystalline solids. Amorphous carbon nitride (a-CN$_{xd}$) and hydrogenated carbon nitride films are expected to be applicable widely as, for example, super hard coating material with low friction coefficient [13-15], low band gap protective material on hard disks and read heads [16, 17], photoluminescence layers [18], carbon nitride nano-tubes [19-20], biosensor [21] and anti–

---

biomaterials [22, 23], or ultra low dielectric constant material [24]. In our previous work, we found that the dielectric constant is around 2.46 in case of amorphous hydrocarbon film (a-HC) deposited by CH_4/Ar DBD plasma process (the work was associated with the incorporation of -CH_3 unit in SiOCH film) [25]. The presence hydrogen eventually induces the extra charging effect on the surface region of the hydrocarbon film. The hydrogen is connected to C or N mostly to weak hydrogen bridging bond or vaan der Waals forces [26]

In this paper we report a comparative study of electronic bond structure and chemical composition of amorphous carbon, hydrocarbon, carbon nitride and hydrogenated carbon nitride film. Three important features have been compared; chemical shift of C 1s peak, bond structure (sp, sp2, sp3, NH etc) and florescence property of the four corresponding films (a-C, a-HC, a-CNx and a-HCNy).

2   EXPERIMENT

2.1. a-C and a-CN$_x$ and samples

a-CNx film is deposited in DC magnetron sputtering system (DC-MS) with the sputtering of a graphite target under different partial pressures (in this case at 5 Pa) of nitrogen gas, that is attached to a high vacuum chamber (base pressure ~ 1×10^{-7} mbar). The film deposited at 5 Pa partial pressure corresponds to the N/C ratios is about 0.41. On the other hand amorphous carbon film was deposited by sputtering of graphite target in Ar buffer gas medium. The a-CN$_x$ films were deposited on a p–type Si (100) substrate which was placed on the ground electrode. The typical film deposition time was 1 hours for all the deposited films. The magnetron discharge power was kept constant for all the measurement at 100 W. Similarly, a-C film is deposited in DC magnetron sputtering system (DC-MS) with the sputtering of a graphite target under different partial pressures (in this case at 5 Pa) of Ar gas, that is attached to a high vacuum chamber (base pressure ~ 1×10^{-7} mbar) [27].

2.2. a-HC and a-HCN$_y$ samples

a-HCN$_x$ film is deposited with CH_4:N_2 gas mixture ratios (1:3) in dielectric barrier discharge plasma. And a-HC film is deposited by CH_4/Ar gas mixture DBD plasma. Both the films were deposited on p–type Si (100) substrate which is placed on the ground electrode. The typical time duration of the film deposition is 1 hours for all the deposited films. The experimental set up of the dielectric barrier discharge has been explained in details elsewhere [ ]. Both the Ag electrodes are covered by dielectrics: the upper (powered) electrode is covered with aluminum oxide (ε ~ 10); the lower (grounded) electrode with a glass plate (ε ~ 3.8). Both electrodes were separated by 0.15 cm from each other. A small piece of Si (100) wafer was placed on the glass electrode. The upper electrode is connected to a home-built high voltage power supply, while the lower electrode is grounded. The chamber is pumped by a membrane pump down to about 10 mbar. Pressure inside the plasma chamber was controlled by two gas flow controllers for methane and nitrogen and by an adjustable needle valve between the chamber and the membrane pump. The experiments were performed with the chamber filled at a pressure of 300 mbar. The amplifier can be operated with maximum power of 500 W. Experiments were performed with the voltage of 10.5 kV (peak–to–peak) and with frequency of 5 kHz. The electrical power under these conditions was 4 W [27].

2.3. Film characterization

The typical film deposition time was 1 hours for all the deposited films. The deposited films have been characterized by three different techniques as follows:

X–ray photoelectron spectroscopy (XPS) measurements of the a-HCNx and a-CNx films were performed on a multi–technique 100 mm hemispherical electron analyser (VSW), using Al $K\alpha$ radiation (photon energy 1486.70 eV) as the excitation source and the binding energy (BE) of Au (Au $4f_{7/2}$: 84.00 eV) as the reference. The XPS spectra were collected in a constant analyser energy mode, at a chamber pressure of 10^{-8} mbar and pass energy of 23.5 eV at 0.125 eV/step [28, 29].

Fourier transform infrared (FTIR) absorption spectra were obtained by means of a FTIR spectrometer Bruker (Vector 22) in transmission mode. The plain sample was placed in a vacuum chamber built inside the spectrometer in order to minimize the IR signal of water vapour, CO_2 content and noise. The measuring signal passed the optical way with an aperture diameter of 3 mm with spectral resolution 4 cm^{-1}. For optimal signal–to–noise ratio 50 scans were averaged per sample spectrum and apodized by applying of the Happ–Genzel apodization function for Fourier transformation. Interferograms were used with zero–filling factor of 0. The background spectrum was independently measured on a pure silicon substrate [28, 29].

Raman spectra were measured on a spectrometer that is oriented as a micro confocal system (Jobin Yvon, Model-LabRAM HR-800). The slit width was 400 μm and the confocal hole was 600 μm in diameter. A 632.18 nm red laser was used as a light source and a CCD as detector. The grating used in the spectrograph was 600 grooves/mm. The objective for focusing the light was 100X while the Raman configuration was in backscattering configuration [28, 29].

3   RESULTS

3.1. X-ray photo electron spectroscopy (XPS)

Figure 1a shows the full scale (260 eV to 1250 eV, with a break at 560 eV to 950 eV) XPS spectrum of a-C, a-HC, a-CN$_x$ and a-HCN$_y$ films. C 1s and O 1s peak on XPS spectrum is the common features for the four spectrums. In the inset of figure 1a, the zoomed area of N 1s peak intensity is illustrated. It shows that N 1s peak in a-HCN$_y$ film is shifted to higher binding energy compare to a-CN$_x$ film.
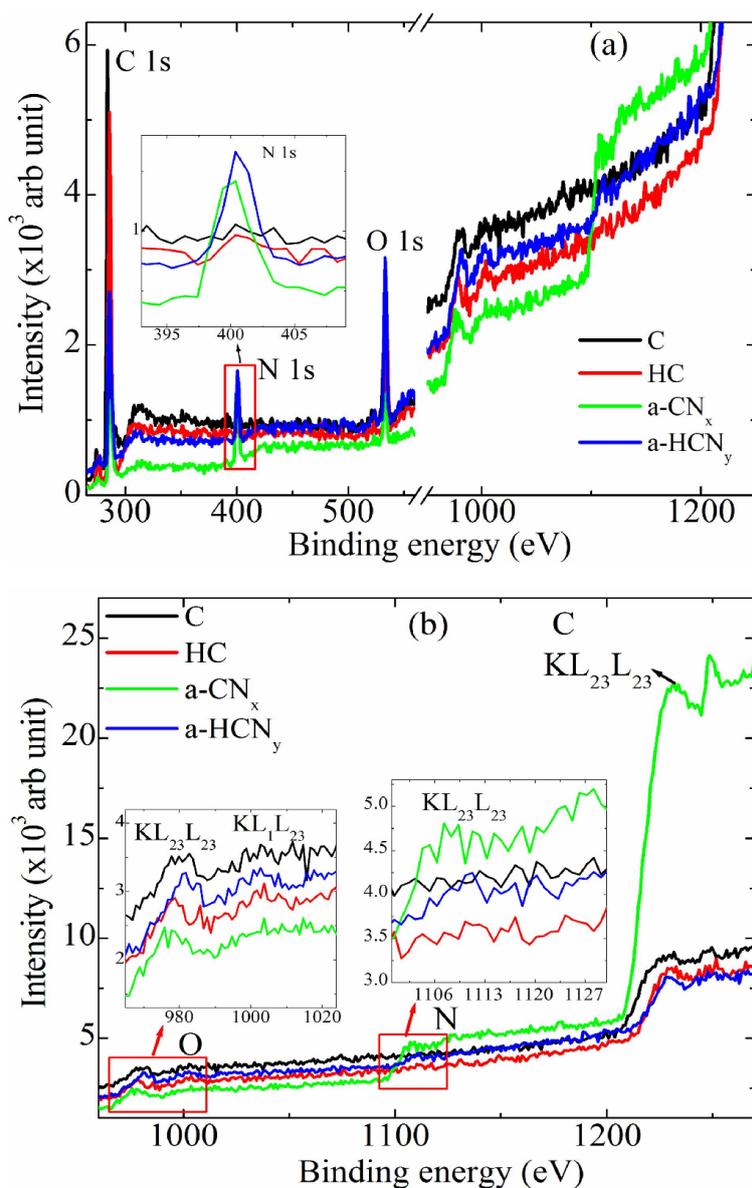
Figure 1. (a) Full scale (260 eV to 1250 eV, with a break at 560 eV to 950 eV) XPS spectrum of a-C, a-HC, a-CN$_x$ and a-HCN$_y$ films. In the inset of figure (a), the zoomed area of N 1s peak intensity is illustrated. (b) Auger lines (951 eV to 1270 eV) of the corresponding films and in the inset the zoomed area of O (KL$_{23}$L$_{23}$, KL$_1$L$_{23}$) and N (KL$_{23}$L$_{23}$) Auger lines are illustrated. The

intensity scales for the all the spectra are not the same. The XPS spectra were obtained with Mg $k\alpha$ X rays at 23.5 eV pass energy at 0.125 eV/step.

Figure 1b shows the Auger peak (or Auger transition) of O 1s (KL$_{23}$L$_{23}$, KL$_1$L$_{23}$), and C 1s (KL$_{23}$L$_{23}$) of the corresponding films. The Auger peak of N (KL$_{23}$L$_{23}$) shows only in a-CN$_x$ and a-HCN$_y$ films. K (1s) is the initial core hole location. L$_1$ (2s), L$_{23}$ (2p) is the origin of relaxing electron and Auger electron (electrons that leaves ion). Auger lines of O 1s and N 1s is shown in the inset the zoomed area of O (KL$_{23}$L$_{23}$, KL$_1$L$_{23}$) and N (KL$_{23}$L$_{23}$) Auger lines are illustrated [30].

The Gaussian fits to the XPS lines resulted in to three or four different peaks for the C−1s line. The general strategy of the data evaluation was identical to those for standard spectroscopic techniques. Si (2p) with a Binding Energy (BE) = 99.3 eV was taken as a reference. The calibration details about this chemical shift are discussed in our previous work. The results shown below were corrected by subtracting the experimentally observed shift for all the analyses. A clear image of the possible chemical bonds between nitrogen and carbon can be deduced from the deconvolution of the individual C−1s, N−1s and O−1s lines into Gaussian-shaped lines. This indicates that the carbon is involved in chemical bonds with nitrogen [29].

Figure 2 shows the C-1s XPS peak of a-C, a-HC, a-CN$_x$ and a-HCN$_y$ films to understand the chemical shift and peak broadening. C 1s peak appears at 283.92 eV, 284.50 eV, 285.79 eV and 286.06 eV in carbon (graphite), a-HC, a-CN$_x$ and a-HCN$_y$ films, respectively. The C1s peak at 283.5 eV is taken as reference [30]. C 1s XPS peak of a-CN$_x$ and a-HCN$_y$ films showing higher chemical shift compare to a-C and a-HC films. The C−1s peak broadens and also becomes more asymmetric as N and H is connected to carbon. This is happens due to the anomalous surface charge distribution of the silicon substrate covered by the carbon film.

Figure 3 shows the XPS C 1s core−level spectra of a-C, a-HC, a-CN$_x$ and a-HCN$_y$ films. The deconvoluted C 1s XPS spectra show three sub-peaks in a-C and a-HC films whereas a-CN$_x$ and a-HCN$_y$ show four sub-peaks. The carbon peak at the binding energy range 283.50–284.5 eV is identified as originating from adventitious (extrinsic or accidental) carbon or graphitic carbon. The C 1s peak binding energy range at 287.38–288.92 eV is identified as originating from CO type bonds which are depending on the type of bonding such as ketones/aldehydes (−CO/−CHO), carboxyls (−COOH) and carbonates (−CO$_3$) [12, 28, 29, 30]. In figure 3 (a) the deconvoluted C 1s XPS spectra of a-C film exhibit three peaks at 283.94 eV, 285.67 eV and 288.37 eV are attributed to adventitious carbon, C=C and CO bonds, respectively. Similarly, C 1s XPS spectra of a-HC film shows three peaks at 284.50 eV, 286.12 eV and 288.79 eV are referred to adventitious carbon, C-H bond and ketones/aldehydes (−CO/−CHO), carboxyls (−COOH) bonds, respectively.
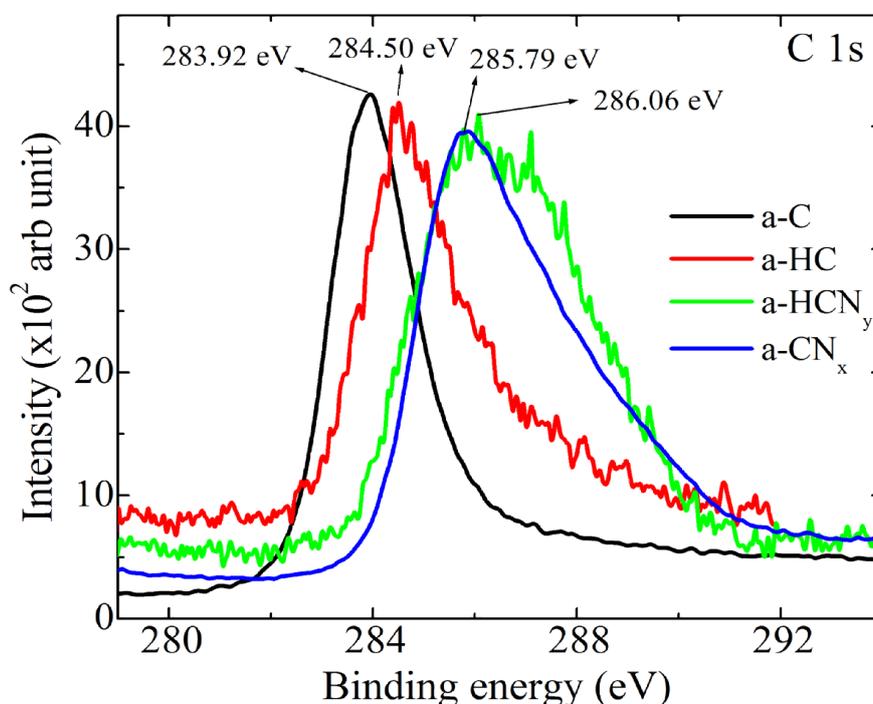
Figure 2. Typical C 1s XPS spectrum of a-C, a-HC, a-CN$_x$ and a-HCN$_y$ films. The intensity scales for the C spectra are not the same.

On the other hand deconvoluted C1s XPS spectra of a-CN$_x$ and a-HCN$_y$ films exhibits four sub-peaks. C 1s XPS peak of a-CN$_x$ exhibits four sub-peaks at 285.74 eV, 287.56 eV, 289.34 eV and 291.53 eV which are assigned to C-C, C-N, C≡N and C-O bonds, respectively. Similarly, four sub-peaks are observed at 285.01 eV, 285.96 eV, 287.41 eV and 289.01 eV in C 1s peak of a-HCN$_y$ films are assigned as C-C, C-N, C≡N and C-O bonds, respectively. The presence of NH group in the XPS of a-HCN$_y$ film is mentioned by most of the previously published literature [12, 28, 29, 30].
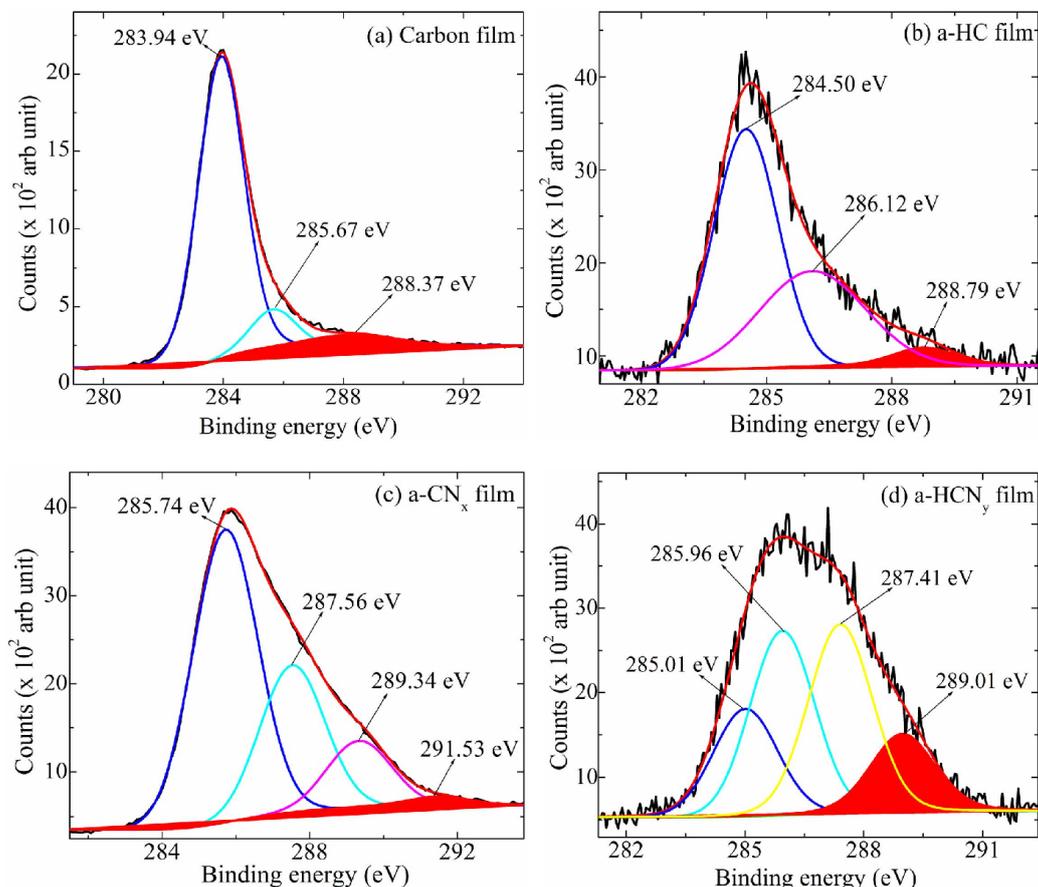
Figure 3. Deconvoluted C 1s XPS spectra of (a) a-C, (b) a-HC, (c) a-CN$_x$ and (d) a-HCN$_y$ films. C 1s XPS spectra obtained with Mg $k\alpha$ x rays at 23.5 eV pass energy at 0.125 eV/step. The red marked peak area is referred as oxide peak. The data are presented after inelastic background subtraction and using Gaussian fits. The intensity scales for the C spectra are not the same.

3.2. FT–IR absorption spectroscopy

FTIR absorption spectra were carried out in the range of 4000–1000 cm^{-1} for all the a–CN$_x$ samples, deposited by DBD technique. The samples were categorized in three groups; a) absence of nitrogen in carbon film, b) presence of hydrogen in carbon film and c) presence of hydrogen and nitrogen in carbon film. Various absorption bands show the presence of N-H & O-H overlapping band (3750–3010 cm^{-1}), sp^3-(CH)$_n$ stretching groups (3000-2800 cm^{-1}), sp^1 –C≡N stretching (2295–2080 cm^{-1}), sp^2 phase associated C=N, C=C and C-N stretching band (1835–1495 cm^{-1}) and C–H$_x$ bending vibration (1480–1365 cm^{-1}) [13, 26, 28, 29]. The assignments of these frequencies to their functional groups were carried out by comparison with the assignments reported in text books and literature [12, 28, 29, 30].

Figure 1, shows the FTIR spectra of a-C, a-HC, a-CN$_x$ and a-HCN$_x$ films measured at room temperature. FTIR of graphite spectra shows the sp^2 phase (-C=C-) structure but there is also a peak associated at 1103 cm^{-1} region is referred as Si-O-Si linkage network. It is due to in-homogeneity of the film surface and bare silicon surface. Such a peak is not observed in rest of the deposited film FTIR spectrum. Amorphous hydrocarbon (a-HC) film shows prominent sp^3 and sp^2 phase at 1803-1300 cm^{-1} and at 2820-3018 cm^{-1}. The peak in the range of 2820 cm^{-1} to 3018 cm^{-1} including two distinguishes sub-peaks. The peak at 2960 cm^{-1} and 2868 cm^{-1} are assigned as CH$_2$ asymmetric stretching vibration and CH$_3$ symmetric stretching vibration,

respectively. It can also be observed that, there is weak shoulder at 2952 cm^{-1} which may be due to CH$_3$ asymmetric stretching vibration [ ]. The absorption band at 3650–3132 cm^{-1} is referred as OH band and it appears due to oxygen adsorption and surface contamination.
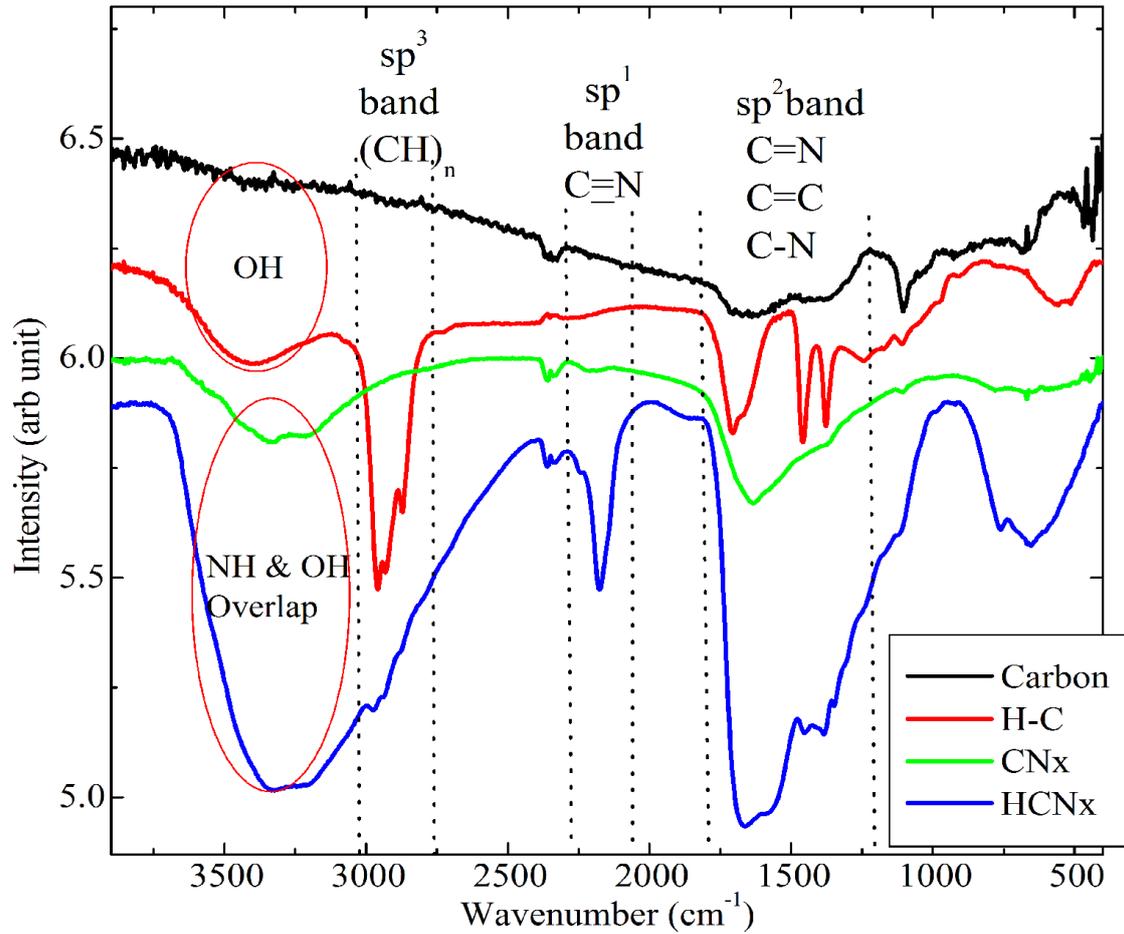
Figure 3. Deconvoluted C 1s XPS spectra of (a) a-C, (b) a-HC, (c) a-CN$_x$ and (d) a-HCN$_y$ films. C 1s XPS spectra obtained with Mg $k\alpha$ x rays at 23.5 eV pass energy at 0.125 eV/step. The red marked peak area is referred as oxide peak. The data are presented after inelastic background subtraction and using Gaussian fits. The intensity scales for the C spectra are not the same.

3.3. Raman spectroscopy
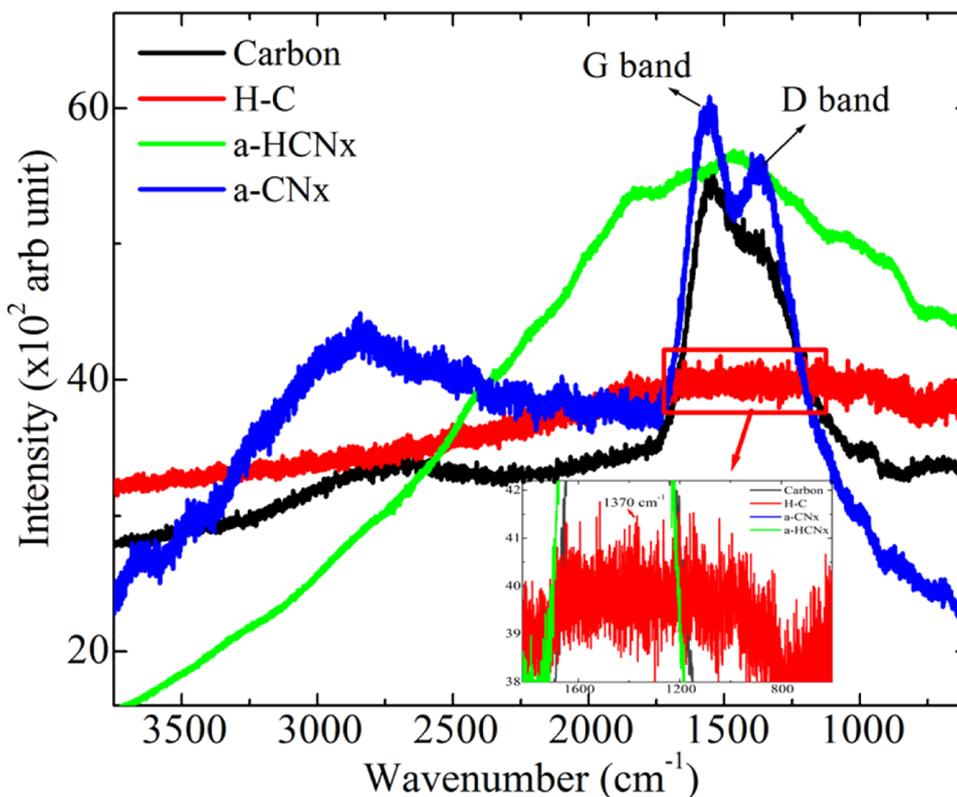
Figure 5. Raman spectra of carbon, a-HC, a-HCN and a-CN film deposited by different plasma deposition methods.

Fig. 2 shows the Raman spectra of a-HCN$_x$ and a-CN$_x$ film deposited at room temperature. A very strong fluorescence effect is observed in the case of the a-HCN$_x$ film. On the other hand, the a-CN$_x$ film shows a similar trend of fluorescence effect with a signature of graphite (G band, 1550 cm^{-1}) and disorder (D band, 1385 cm^{-1}) bands. The broad band at 2870 cm^{-1} might go back to NH/OH surface groups with strong hydrogen bonds. CH$_2$/CH$_3$ bands should be less broad and are also IR active but were not observed in the IR spectra of a-CN$_x$ films (see above). Several oscillations were observed in the spectrum from 1800 cm^{-1} to 2700 cm^{-1} and 3400 cm^{-1} to 3600 cm^{-1}.

It was expected that the G band (sp^2 ordered) would dominate over the D band (sp^2 disordered) but in reality it did not show any big difference in the shifting with N concentration. In the case of a-C film, the graphite (G band, 1550 cm^{-1}) band is visible prominently with a distinguishable hump of a disorder (D band, 1385 cm^{-1}) band. But in the case of a-HC film the signature of G and D bands are seen with fluorescence effect.

4   DISCUSSION

The spectroscopic analyses suggest that the presence of oxide layer is not only the prime cause but the presence of nitrogen is partially responsible for the chemical shift towards higher binding energy. In x-ray photoelectron spectroscopy (XPS), C 1s spectra of a-HCN$_y$ film shows higher chemical shifts compare to a-C, a-HC and a-CN$_x$. Raman spectra display a strong fluorescence effect of a-HC and a-HCN$_y$ where as a-C and a-CNx exhibits a promising G and D band at room temperature. Fourier transform infrared spectroscopy (FTIR) spectra show a large NH-OH over lapping region in a-HCN$_y$ compare to a-HC and a-CN$_x$ film whereas it is negligible in a-C. FTIR spectra show that the a-C, a-HC and a-CN$_x$ films are dominated by sp^2 bonded region while a-HCN$_y$ is the mixture of sp^2, sp^3 and hydrogen bridging bond.

In fig 1b, Auger lines of KL$_1$L$_{23}$ represent the Auger electron emitted from 2p orbital level. At the initial stage the incident x-ray/photon kick out one electron from K shell and to fill this core hole position one electron from L$_1$ (2s) orbit jump to K (1s) shell orbit. Due to this jump of electron from higher shell to lower shell the emitted energy enhance to kick another electron from L$_{23}$ shell which is called Auger electron. Similarly, in case of KL$_{23}$L$_{23}$ peak represent the Auger electron emitted from 2p orbital level. Here the electron jump from 2p orbital (L$_{23}$) to K shell orbit to fill the initial core hole position. In this case the

emitted energy enhance to kick another electron from same orbital (2p) which is denoted as Auger electron of $KL_{23}L_{23}$ transition. Fig 2 shows that the nitrogen connected film exhibit higher chemical shift and here C1s peak appears at higher binding energy in XPS spectrum of a-CN_x and a-HCN_y films compare to the a-C and a-HC. Ofcourse there is oxygen contamination at the surface but it is common to all of the four films.

It is observed from fig 2 that the a-C and a-CN_x films (deposited in dc magnetron plasma) exhibit smooth C 1s curve where as a-HC and a-HCN_y films (deposited in DBD plasma) show the noise signal in the XPS spectrum. DBD films are highly porous and composed with island growth and it exhibits insulating property [CPL]. The presence hydrogen could induce the extra charging effect on the surface region of the film. The hydrogen is connected to C or N mostly to weak hydrogen bridging bond or vaan der Waals forces. As the film is exposed to the air the surface contamination take place and oxygen sit top of the surface by adsorption process and sometimes it reaction with the existing hydrogen (NH group) by weak interaction forces and for 'OH' bridge. The noise signal in XPS measurement happened due to surface charging effect, which means the surface electron are not flowing properly to complete the circuit. Even thin film can show such noise signal if there is hydrogen or oxygen present in the film [29].

All the four films have sp2 phase in common but there structure is different. Hydrocarbon film shows three different peaks (1705.16 cm^{-1}, 1458.22 cm^{-1} and 1377.13 cm^{-1}) where as amorphous carbon shows dominating graphitic band at named G (1630.21 cm^{-1}) and disordered D (1377.12 cm^{-1}) band in sp2 region. There are some common features in case of a-CN_x and a-HCN_x film regarding the sp1, sp2 and sp3 phases at room temperature, but they behave differently when they are annealed. Both show the NH-OH overlapped region at 3750–3010 cm^{-1}. The intensity of nitrile group (−C≡N) in a-CNx is very small compare to a-HCN_x film. The decrease in the intensity of the C-H stretching vibrations and the increase in the number of N-H stretching vibrations may be caused by the increase in the nitrogen content in the film where NH_n group gradually replaces the CH_n group and C=C becomes more active. The NH-OH overlapped tail is long enough up to 2500 cm^{-1} due to the presence of volatile phase and Hydrogen Bridge formed in between two molecular chains. This long tail absorption band is removed as annealing temperature approaches to 300 ^{0}C. The hydrogen bridge bonding breaks up due to heating and figure 3 (a) shows that the NH -OH overlapped tail is reduced and it end up with a band of 2950 cm^{-1} to 3570 cm^{-1}. Both a-CNx and a-HCNx film have common features regarding the sp^2 and sp^1 phases at room temperature. Both show the NH-OH overlapped region at 3650–3010 cm^{-1}. The intensity of nitrile group (−C≡N) in a-CNx is very low compare to a-HCNx film. a-HCNx shows a intense finger print region (1660 cm^{-1} to 1300 cm^{-1}) compare to a-CNx film. a-CNx and a-HCNx shows higher chemical shift compare to a-HC, a-C film. It is obvious that the presence of nitrogen is causing the extra chemical shift towards higher binding energy region. The electronegativity of O is about 3.56 where as N has 3.

5 CONCLUSION

The direct observation of our spectroscopic results (Fig 1-3) depict that the chemical shift (or binding energy shift towards higher region) of C 1s peak gradually increase successively from a-HC, a-CNx and a-HCNy film where graphite peak is taken as reference. The four corresponding films are deposited in oxygen free environment but there is 5 to 10% oxygen is present in those films due to adsorption or absorption at top layer. C 1s XPS spectra of a-HCNy film exhibit highest chemical shift out the four. a-CNx and a-HCNx shows higher chemical shift compare to a-HC, a-C film. It is obvious that the presence of nitrogen is causing the extra chemical shift towards higher binding energy region. Chemical shifts of C 1s peak is about 2.1 eV and 1.3 eV in XPS of a-HCNx and a-CNx film at room temperature, respectively. The fluorescence effect is due to the presence of organic matrix (Chemfors, NH, nitrile, C=N etc) in the deposited solid.

REFERENCES

[1]   J. C. Angus, P. Koidl, and S. Domitz, in Plasma Deposited Thin Films, edited by J. Mart and F. Jansen (CRC, Boca Raton), p. 89. 1986.

[2]   P. Koidl, Ch. Wild, B. Dischler, J. Wagner, and M. Ramsteiner, Mater. Sci. Forum, vol. 52/53, pp. 41, 1989.

[3]   J. Robertson, Surf. Coat. Technol. Vol. 50, pp. 185, 1992.

[4]   J. L. Bredas and G. B. Street, J. Phys. C vol. 18, pp. L651, 1985.

[5]   J. Robertson and E. P. O'Reilly, Phys. Rev. B vol. 35, pp. 2946, 1987.

[6]   A. C. Ferrari and J. Robertson, Phys. Rev., B vol. 61, pp. 14095, 2000.

[7]   C. Hopf, W. Jacob, A. von Keudell, J. Appl. Phys., vol. 97, pp. 094904, 2005.

[8]   T. Schwarz-Selinger, M. Meier, C. Hopf, A. von Keudell, W. Jacob, Vacuum, vol. 71, pp. 361, 2003.

[9]   W. Jacob, Thin Solid Films, vol. 326, pp. 1, 1998.

[10] E. Salancon, T. Dürbeck, T. Schwarz-Selinger, F. Genoese, W. Jacob, J. Nucl. Mater., vol. 376, pp. 160, 2008.

[11] A. Y. Liu, M. L. Cohen, Science, vol. 245 pp. 841, 1989**.**

[12] D. Marton, K. J. Boyd, A. H. Al–Bayati, S. S. Todorov, and J. W. Rabalais, Phys. Rev. Lett. Vol. 73 pp. 118, 1994.

[13] N. Hellgren, M.P. Johansson, E. Broitman, L. Hultman, J.E. Sundgren, Phys. Rev. B, vol. 59, pp. 162, 1999.

[14] D. Li, Y.W. Chung, M.S. Wong, W.D. Sproul, J. Appl. Phys., vol. 74 pp. 219, 1993.

[15] H. Yao, W.Y. Ching, Phys. Rev. B, vol. 50 pp. 11231, 1994.

[16] A. Mansour, D. Ugolini, Phys. Rev. B, vol. 47 pp. 10201, 1993.

[17] J. Robertson, Thin Solid Films, vol. 383 pp. 81-88, 2001.

[18] Zambov, L. M; Popov, C.; Abedinov, N.; Plass, M. F.; Kulisch, W.; Gotszalk, T. *Adv. Mater.*, 12 (2000) 656–660

[19] Wang J, Miller D R, Gillan G, Chem. Commun., vol. 19 pp. 2258-2259, 2002.

[20] Plass M. F, Popov C, Ivanov B, Mandl S, Jelinek M, Zambov L. M, *Appl. Phys. A*, vol. 72 pp. 21–27, 2001.

[21] Sung Pil Lee**,** Sensors, vol. 8 pp. 1508–1518, 2008.

[22] Majumdar A, Schröder K and Hippler R, J. Appl. Phys*.,* vol. 104 **pp.** 074702, 2008.

[23] A. Majumdar, Ramesh Ummanni, Karsten Schröder, Reinhard Walther, and Rainer Hippler, J. Appl. Phys., vol. 106 pp. 034702, 2009.

[24] Abhijit Majumdar, Sadhan Chandra Das, Thoudinja Shripathi, Rainer Hippler, Chem. Phys. Lett. , vol. 524 pp. 62-67, 2012.

[25] A. Majumdar, G. Das, N. Patel, P. Mishra, D. Ghose, and R. Hippler, J. Electrochemical Society*,* vol. 155 no. 1 pp. D22-D26, 2008.

[26] J. Houska 1, J.E. Klemberg-Sapieha, L. Martinu, Surf. Coat. Technol., vol. 203 pp. 3770–3776, 2009.

[27] Majumdar, A. and Hippler, R. *Rev. Sci. Instrum*., Vol. 78 pp. 075103–075108, 2007.

[28] A. Majumdar, G. Das, K.R. Basvani, J. Heinicke, R. Hippler, J. Phys. Chem. B, vol. 113 pp. 15734, 2009.

[29] Majumdar, A.; Schäfer, J.; Mishra, P.; Ghose, D.; Meichsner, J and Hippler R. *Surf. Coat. Technol.*, vol. 201 pp. 6437, 2007.

[30] John, F. Moulder et al. *Handbook of X–ray Photoelectron Spectroskopy*, Perkin–Elmer Corporation, 1992.